Hydrol. Earth Syst. Sci. Discuss., 10, 12331–12371, 2013
www.hydrol-earth-syst-sci-discuss.net/10/12331/2013/
doi:10.5194/hessd-10-12331-2013

Hydrology and Earth System Sciences Discussions
Open Access

Variability of extreme precipitation over Europe and its relationships with teleconnection patterns

A. Casanueva[1], C. Rodríguez-Puebla[2], M. D. Frías[1], and N. González-Reviriego[2]

[1]Grupo de Meteorología, Dpto. Matemática Aplicada y Ciencias de la Computación, Univ. de Cantabria, Avda. de los Castros, s/n, 39005 Santander, Spain
[2]Dept. of Atmospheric Physics, Plaza de la Merced S/N, University of Salamanca, Salamanca, Spain

Received: 4 September 2013 – Accepted: 1 October 2013 – Published: 15 October 2013

Correspondence to: A. Casanueva (ana.casanueva@unican.es)

Published by Copernicus Publications on behalf of the European Geosciences Union.

Abstract

A growing interest in extreme precipitation has spread through the scientific community due to the effects of global climate change on the hydrological cycle and their threat on natural systems more than averaged climatic values. Understanding the variability of hydrological indices and their association to atmospheric processes could help to project the frequency and severity of extremes. This paper evaluates the trend of three precipitation extremes: the number of consecutive dry/wet days (CDD/CWD) and the quotient of the precipitation in days where daily precipitation exceeds the 95th percentile of the reference period and the total amount of precipitation (or contribution of very wet days, R95pTOT). The aim of this study is twofold. First, extreme indicators are compared against accumulated precipitation (RR) over Europe in terms of trends using non-parametric approaches. Second, we analyse the geographic opposite trends found over different parts of Europe by considering their relationships with large-scale processes, using different teleconnection patterns. The study is accomplished for the four seasons using the gridded E-OBS dataset developed within the EU ENSEMBLES project.

Different patterns of variability were found for CWD and CDD in winter and summer, with north-south and east–west configurations, respectively. We consider physical factors to understand the extremes variability by linking large-scale processes and hydrological extremes. Opposite association with the North Atlantic Oscillation in winter and summer, and the relationships with the Scandinavian, East Atlantic patterns and El Niño/Southern Oscillation events in spring and autumn gave insight into the trend differences. Significant relationships were found between the Atlantic Multidecadal Oscillation and very extreme precipitation (R95pTOT) during the whole year. The largest extreme anomalies were analysed by composite maps using atmospheric variables and sea surface temperature. The association of extreme precipitation indices and large-scale variables found in this work could pave the way of new possibilities for the projection of extremes in downscaling techniques.

1 Introduction

The occurrence of extreme events and their impacts on society have become a fundamental issue due to the great climate change effects on them rather than those on mean values causing, for example, damages related to health, agriculture, energy and tourism. Broad knowledge about extremes would allow a better adaptation to new climate conditions and reduce the damage of climate change (IPCC, 2011). Heat and cold waves, very heavy precipitation episodes and droughts are examples of climate extremes related to the tails of frequency distributions. Other definitions of climate extremes refer to the occurrence of a variable above (or below) a threshold. The predictions announced by the IPCC (Intergovernmental Panel on Climate Change) reports (IPCC, 2011) indicate that extreme events are very likely to change in intensity, frequency and location in 21th century (see e.g. Easterling et al., 2000; Tebaldi et al., 2006). This IPCC report points out the human influence as a likely cause of global warming and changes in the hydrological cycle, with a precipitation decrease in subtropical areas and extremes intensification (Trenberth, 2011). The interest about monitoring extreme events is addressed in Donat et al. (2013) and Peterson et al. (2013) that compared results of the indices for different gridded datasets for the whole globe and for US, respectively. At a regional scale, the Mediterranean and North Eastern European regions have been identified as primary climate change hot-spots (Giorgi, 2006), which motivates the study of extremes in this continent. Since climate extremes have occurred throughout history (Schonwiese et al., 2003; Tank and Konnen, 2003), individual extremes can not be simply and directly attributed to anthropogenic climate change because they can be included in the limits of the broad natural variability. However, the changes in the frequency of climate extremes may be related to global warming due to variations and shifts of atmospheric circulation. van den Besselaar et al. (2012) shows different trend patterns over Europe depending on the season, highlighting the need of linking precipitation extremes to atmospheric flow patterns.

HESSD
10, 12331–12371, 2013

Although extreme indicators have been widely used to analyse extreme events in different regions over Europe (see e.g. Schonwiese et al., 2003; Kostopoulou and Jones, 2005; Hidalgo-Muñoz et al., 2011), here we present the study for the entire continent and try to relate the opposite trends in different regions with teleconnection patterns; therefore, we examine the impact of large-scale variables on extremes to have some criteria for the statistical downscaling of extremes under a warming climate. Moreover, we compare mean precipitation to precipitation extreme indices.

Teleconnections refer to associations of climate system anomalies, both atmospheric and oceanic, that take place in long distances (Barnston and Livezey, 1987). They govern the variability of the climate system in different spatial and temporal scales, being one important issue for the atmospheric science. Several Northern Hemisphere teleconnection patterns are considered in this study in order to find associations with the precipitation extremes over Europe: the North Atlantic Oscillation (NAO), the Scandinavian Pattern (SCAND), the East Atlantic Pattern (EA) and the East Atlantic/Western Russia Pattern (EAWRUS). Also the Southern Oscillation Index (SOI) and the Atlantic Multidecadal Oscillation (AMO) were taken into account due to their interannual and decadal oscillations. These teleconnection patterns have been related in the literature to common atmospheric variables such as temperature and precipitation, but also to river flows, snow cover or cereal production (see e.g. Rodriguez-Puebla et al., 2007; Carril et al., 2008; Vicente-Serrano et al., 2009).

The aim of this study is twofold, on one hand we describe the main features of the precipitation extremes in Europe using indicators derived seasonally from E-OBS dataset (Haylock et al., 2008). On the other hand we consider some processes of the atmospheric circulation by linking teleconnection patterns with hydrological processes in order to explain the non-stationarity of extremes. Firstly, a statistical descriptive study and a trend analysis of precipitation extreme indicators are calculated over the entire Europe. Secondly, we try to interpret the opposite trend patterns found over different European regions by considering their relationships to the main modes of circulation variability.

The manuscript is structured as follows. In Sect. 2 we describe the data and in Sect. 3 the methodology applied. Main results are presented in Sect. 4 for each season. Comparison of different results and main conclusions are presented in Sect. 5.

2 Data

2.1 Precipitation data

Daily precipitation data from the E-OBS dataset (version 5.0) were used with resolution 0.5°, for the period from 1950 to 2010 (Haylock et al., 2008; Hofstra et al., 2009). This dataset has been developed within the framework of the EU ENSEMBLES Project (http://www.ensembles-eu.org) and represents the first freely available daily data with very high resolution covering Europe. This dataset has been obtained by interpolation of observed data from more than 2300 stations over Europe. It presents advantages with respect to previous products because of the higher spatial resolution, the time and spatial coverage and the larger number of stations used. Particularly, this version increases the number of stations in Spain and Germany, with respect to the previous one.

2.2 Teleconnection patterns

In this study, the variability of extremes over Europe is related to different Northern Hemisphere teleconnection patterns: the Arctic Oscillation (AO), the North Atlantic Oscillation (NAO), the Scandinavian Pattern (SCAND), the East Atlantic Pattern (EA) and the East Atlantic/Western Russia (EAWRUS). Also the Southern Oscillation Index (SOI) from the Tropical Pacific and the Atlantic Multidecadal Oscillation (AMO) have been found to affect precipitation. The behavior of these teleconnection patterns changes during the year. For instance, the summer NAO differs significantly from the winter and spring pattern, and also the leading Empirical Orthogonal Function (EOF) mode

HESSD
10, 12331–12371, 2013

of the summer precipitation has a spatiotemporal structure which is principally different from those of the winter and spring seasons (Zveryaev, 2006). According to this, it seems appropriate to analyze the relationships between teleconnections and precipitation seasonally.

It is widely known that the NAO modulates precipitation in Europe (see e.g. Trigo et al., 2004; Zorita et al., 1992), and particularly, it justifies most of the interannual variability of winter precipitation over Spain (Rodriguez-Puebla et al., 2001) and also affects the intensity and frequency of extreme precipitation in different regions over the Iberian Peninsula (Vicente-Serrano et al., 2009). The NAO mostly explains the precipitation variability in Europe, nevertheless there are other modes of variability such as the EAWRUS, the SCAND or the EA (Ramos et al., 2010) which are also related. For instance, Bueh and Nakamura (2007) found that the positive SCAND phase causes a decrease in fall precipitation over northeastern Europe. The EA pattern is widely described in Wallace and Gutzler (1981), and Rodriguez-Puebla et al. (2001) shows the important role of the EA and EAWRUS to explain the precipitation variations in the northern part of the Iberian Peninsula in winter. We also include one global index on Tropical Pacific, the SOI. This atmospheric index is related to El Niño Pattern, which consists on the first mode of variability of the global sea surface temperature. It is responsible of the precipitation regime not only in the Central and Eastern Pacific, it is also related to droughts in Brazil and Australia, the Indian monsoon and the flow of the Nile River (see e.g. Ropelewski and Halpert, 1987; Hoerling and Kumar, 2000). Moreover, Rodo et al. (1997) and Frias et al. (2010) have related this index to the precipitation in the Iberian Peninsula in spring and autumn. Finally, we also considered an oceanic teleconnection pattern: the AMO (Enfield et al., 2001; Dima and Lohmann, 2007). Apart from its relation to precipitation in North America, the AMO warm phase reinforces the Indian and Sahel monsoons and the cyclonic activity in the North of the Atlantic (Zhang and Delworth, 2006).

HESSD
10, 12331–12371, 2013

The time series of these indices were obtained from the Climate Prediction Center (CPC) and the NCEP NOAA web site (http://www.cpc.noaa.gov/data/) for the same period as the E-OBS data.

To attribute the causes of the largest or most significant precipitation extremes we have also considered the sea level pressure and wind at the surface, and velocity potential at 200 hPa level from the NCEP/NCAR reanalysis data (Kalnay et al., 1996), since teleconnection patterns affect the atmospheric conditions at different levels. The velocity potential is computed from horizontal winds at 200 hPa and as shown bellow, it identifies regions where there is converging (diverging) winds and consequently subsidence (rising air) and less (high) precipitation.

3 Methodology

3.1 Extreme indicators

Within the framework of the World Meteorological Organization, the Expert Team on Climate Change Detection and Indices (ETCCDI, http://etccdi.pacificclimate.org/indices_def.shtml), deals with the definition of climate extremes in order to obtain comparable results in different countries. Here we address the study of some hydrological extreme indices derived from precipitation for the four seasons: winter (DJF), spring (MAM), summer (JJA) and autumn (SON) due to different influence through the year. Table 1 shows the indicators considered in this study.

Although there are other hydrological extreme indices, here these three indicators were chosen because they are useful to represent both dry (CDD) and wet (CWD, R95pTOT) conditions. As CDD and CWD are related to the precipitation occurrence, they can characterize droughts indirectly which are of great interest, for instance, for agricultural activities. Moreover, R95pTOT determines the intensity for very heavy events, examining the contribution of the 5 % more extreme days to the total precipitation, which in the case of Spain clearly separates the different extreme-regimes of the Atlantic and Mediterranean climates. This index quantifies very extreme events, which can be responsible for floods and soil erosion. In addition, these three indicators are related to different driving mechanisms. As presented in the following sections, CWD and CDD are more related to large-scale atmospheric circulation while R95pTOT has a convective origin and depends more on local processes and moisture fluxes.

3.2 Trend analysis

The E-OBS data were first analyzed by means of a basic statistical description in order to explore the data distribution. The results of the statistical properties allow us to infer regions more sensitive to suffer changes in climate stationarity. Then, a trend analysis was performed using the Mann–Kendall's test (Kendall, 1975) together with the Sen's test (Sen, 1968). The former test allows to investigate long-term trends of data without assuming any particular distribution and it is less influenced by outliers as it is a nonparametric test. The latter is based on the Kendall's rank correlation tau and it is calculated as the median of the set of slopes joining pairs of points. On one hand, the Sen's slope estimates the magnitude of the variable–time relationship by means of a nonlinear procedure, and, on the other hand, the Mann–Kendall's test (Z Kendall's coefficient) gives us the significance of the trend.

The resulting dipolar structures of the trend patterns are expected to reflect the different influence of atmospheric circulation. Therefore, we consider the relationships between precipitation (mean and extreme) and the teleconnection patterns to give insight into the physical causes for that long-term variation.

3.3 Relationship with teleconnection indices

The Empirical Orthogonal Functions (EOFs) method is applied to identify spatial and temporal variability (Jolliffe, 2002; Wilks, 2006). Lorenz (1956) was the first applying this mathematical artefact to meteorological studies. The EOFs are parameters of the

HESSD
10, 12331–12371, 2013

covariance matrix of data anomalies. Different procedures can be used to calculate the eigenvectors and eigenvalues (von Storch and Zwiers, 1999). In this study, we apply the Principal Component Analysis (PCA) to time series of extreme indicators (and also mean precipitation) in order to characterize extremes by regions. As a result, the first EOFs are the spatial patterns corresponding to the places with the highest variability and the associated scores or Principal Components (from now on denoted as PCs) are the time series related to these places (i.e. PC1 corresponds to EOF1 and so on). This analysis also provides the variance or eigenvalue associated to each PC. We focus the study on the first and second modes of variability, since they are separated (in terms of explained variance) (North et al., 1982) and can be physically interpreted when they are compared to the teleconnection patterns as shown below.

This part of the study remarks the relevance of analysing the influence of teleconnection patterns on hydrological extremes to find the explanations for their variability and, hence, to justify the different trend patterns found in the extremes. Due to the limitations of global climate model outputs for hydrological applications, this work could pave the way of new possibilities for the projection of extremes. Thus, if the precipitation variability can be associated to teleconnection patterns, they would be useful to project extremes changes under other climatic conditions.

4 Results

The spatial distribution of the extreme indicators (Fig. 1) is first analyzed using the E-OBS dataset for every season (by columns) and for the period of study (1950–2010). The highest values of CDD (first row) are found in the Mediterranean Basin, especially in the Iberian Peninsula and Greece in every season. The places with the highest number of CWD (second row) are similar to those with more RR, included as Fig. S1 in the Supplement. The maps for R95pTOT (third row) present the highest values in the south of the continent, especially in the southwestern Iberian Peninsula in summer

Discussion Paper | Discussion Paper | Discussion Paper | Discussion Paper |
HESSD
10, 12331–12371, 2013
Extreme precipitation and teleconnections in Europe
A. Casanueva et al.

and in the whole Mediterranean Basin in the other seasons. The standard deviation (contour lines) is always higher in the places with more (mean or extreme) precipitation.

The comparison of the trend tests for daily mean precipitation (RR) and the three extreme indicators (CDD, CWD and R95pTOT) and the regionalization by using the EOF analysis are shown in the following sections for each season: winter, spring, summer and autumn.

4.1 Winter

Figure 2 shows the results from the *Z* and Sen trend tests for RR, CDD, CWD and R95pTOT in winter. The triangle size is proportional to the significance, upward-pointing triangles (downward-pointing triangles) indicate positive (negative) trend. With this convention, blue (red) always means wetter (drier) conditions. Only significant trends at 5 % significance level are presented. Black contour lines represent Sen's slope multiplied by 10, in order to express decadal changes. They indicate the mm day^{-1} for RR, days for CDD and CWD and percentage of days for R95pTOT that the index increases or decreases per decade.

Winter precipitation tends to decrease in some areas in the south but increases significantly in the north, which is in agreement with van den Besselaar et al. (2012). However, very extreme precipitation (R95pTOT) tends to increase in sparse areas in the north, center and south of the continent. The number of CWD tends to decrease especially in the Iberian Peninsula and increase in the north-east of the continent, while the increase of the number of CDD extends to the whole Mediterranean Basin. More significant trends were found for extremes than those for mean precipitation.

Due to the dipolar structures found in CDD, CWD and RR trends, the analysis of extremes is here related to teleconnection patterns to connect extremes variability to modes of low frequency variability. These relationships are first analyzed in terms of correlation between the teleconnection indices and the leading Principal Components (PCs) of the extreme indices. Results derived from this approach allow us to choose the teleconnection patterns that mainly influence the extreme precipitation over Europe.

HESSD
10, 12331–12371, 2013

The correlation values obtained for winter are presented in Table 2. These values are calculated for the data without trend to avoid the overestimation of the correlation coefficients due to the trend effect. Values in brackets show the variance of each PC (in %).

In winter, the first PC for both mean and extreme precipitation (CDD and CWD) shows the highest correlation with the NAO. Some other significant correlations have been found between the EA, EAWRUS and SCAND patterns and upper order PCs. Another interesting outcome is that we found the highest relation for the very extreme precipitation (R95pTOT) with the Atlantic Multidecadal Oscillation (AMO). Since this kind of extreme events must depend on convective precipitation more than on large-scale precipitation, it is reasonable to be modulated by this oceanic index, rather than the usual winter circulation regimes. Notice that especially for winter, the explained variance by the PC1 for RR is higher than that for the extremes, since it varies with greater spatial coherence. Haylock and Goodess (2004) previously noted that the variance for the extreme indicators compared with mean values is lower because of the noisier nature of extremes and the large region under study.

Correlation maps for the most significant relationships found in Table 2 are analyzed in more detail. Figure 3 (shadings) shows the correlation values (×100) between the NAO, the EAWRUS and the EA (in rows) with winter RR, CDD and CWD (in columns). Only significant values at 5 % significant level are shown. Contour lines represent the EOF associated to the PC with significant correlation in Table 2 (e.g. the upper left map shows the spatial correlation between the RR and the NAO in shaded and contour lines represent the first EOF (EOF1) from the RR, while the lower left map shows the spatial correlation between the EA and the RR in shaded and the contour lines represent the second EOF (EOF2) from the RR). Note that positive EOF patterns are plotted with solid lines and negative EOF with dashed lines. A north-south dipole of correlation values with the NAO is observed over Europe. Same dipole is shown by the main pattern (EOF1 representing the variance of RR, CWD and CDD). The NAO is negatively correlated to the RR and CWD in the south of the continent and positively in the north, while the EOF1 from RR and CWD are negative in the north and positive in the south. The opposite behavior is found for CDD (Fig. 3, first row, third column). Therefore, positive phases of the NAO cause heavier precipitation and an increase in CWD (decrease in CDD) in the north of Europe and the opposite in the south of the continent. The contrary would happen for negative phases. The correlation of these variables with the EAWRUS is shown in Fig. 3 (second row). Also in this case the EOF1 (contour lines) fits the significant correlated areas (shaded regions). The correlation with this pattern is negative (positive) for RR and CWD (CDD) in the south and the British Isles whereas the opposite is found over Norway. The positive EOF2 of RR (contour lines in Fig. 3, third row, first column) discriminate the Atlantic Basin of the continent and that fits with the region where the RR and EA are more related, in particular, positively associated. Then, positive phases of the EA mean more precipitation (mean and extreme) in those areas. R95pTOT presents positive correlation with the AMO; so positive phases of AMO would increase very extreme precipitation in sparse regions of the continent. The EOF1 of this extreme index does not show any regionalization, so this figure is not shown for any season.

The north-south dipole found for the correlation with the NAO and EAWRUS agrees with spatial structure found in the trend analysis, meaning that teleconnections could be influencing the trend of CDD, CWD and RR besides other interannual variability. To support this idea, we examine the atmospheric processes contributing to the variability of CDD and CWD by grouping the years when their principal components have values greater and lower than the mean plus (minus) the standard deviation (std) multiplied by 1.5. Thus we consider, approximately, 10 % of data as most anomalous extremes. For those years the composite maps of sea level pressure (SLP) and velocity potential at 200 hPa are shown in Fig. 4 for the case of CWD (first row), since this extreme shows greater decreasing trend in a large area over south-center Europe. It was found a dipolar structure with negative SLP anomalies over south western Europe and positive anomalies over subpolar areas. At upper levels we obtain negative values for velocity potential, that means divergence winds over Europe. This atmospheric properties are occurring during NAO negative phases in agreement with results depicted on Table 2. Figure 4c and d shows the composite maps of SLP and velocity potential corresponding to the years with the largest anomalies of the NAO or when the index exceeds the mean ±1.5 std. There is correspondence between the positive and negative anomalies of Fig. 4a and c. At upper levels there is also agreement between Fig. 4b and d with negative and positive velocity potential, respectively. These figures confirm the opposite relationships between NAO and CWD, providing sources of CWD predictability that arises from the links between extremes and low and upper level atmospheric variables.

4.2 Spring

Less significant trends are obtained for spring than for winter RR, CDD and CWD (Fig. 5). In spite of the smaller trends found in sparse regions, they give insight into the noth-south dipolar structure. Increasing trends as important as in the previous section are found for R95pTOT.

The EOF analysis is applied to regionalize the extreme indices and to explain their variability considering the association with the teleconnection patterns. In spring, the SCAND, EA or SOI indices play a more relevant role than the NAO. Table 3 shows that RR, CDD and CWD are more related to the SCAND, but also to the SOI, while the R95pTOT is again more influenced by the AMO.

Figure 6 extends the information presented in Table 3. The second EOF of RR, CWD and CDD (contour lines in Fig. 6, first row) marks a northeast–southwest dipole in the continent. These regions fit quite well with the places where there is a significant correlation with the SCAND pattern (first row, shading). Shaded regions reveal that positive phases of the SCAND would be associated to more precipitation and more CWD (less CDD) in the Iberian Peninsula, Italy and Greece and less precipitation in Norway. Notice that the area affected by the CDD in Scandinavia is bigger than that area related to CWD, but with opposite sign. The EA also affects RR and CWD in spring (Fig. 6, second row), especially in the Atlantic Basin; however, no significant

HESSD
10, 12331–12371, 2013

relation was found for CDD. The SOI is also linked to mean and extreme precipitation (Fig. 6, third row), with positive correlation in the Iberian Peninsula (negative for CDD). This means that La Niña events are associated to wetter springs in this area.

In spring (Fig. 7) the physical processes that cause extreme values of CDD and CWD correspond to a dipolar structure of SLP with centers over Scandinavian and Iberian Peninsula. Figure 7a shows the composite pattern of SLP and wind that causes extreme values of the PC2 of CWD in spring. This configuration resembles the Scandinavian pattern derived for the years with largest anomalies of SCAND (Fig. 7b).

4.3 Summer

For summer (Fig. 8), the mean precipitation decreases (increases) in the west (east) part of the continent (in agreement with van den Besselaar et al., 2012). In this season, the most interesting results concern extremes, especially the CDD that increases significantly in southern France and north of Italy. CWD suffers a decrease in the center and R95pTOT increases over the whole continent, especially in the North.

The correlation analysis of the main PCs from the extremes and the teleconnections (see Table 4) shows that the most important relationship for RR, CDD and CWD is found with the NAO also in this season, although with opposite sign to that in winter. This could be due to changes in the spatial configuration of the NAO pattern in summer with respect to winter (Bladé et al., 2012), since in summer the positive center of this index moves towards northeastern areas. The second PC of these three variables is related to the SCAND pattern. For the very extreme precipitation (R95pTOT), the highest correlation is found again with the AMO, although significant values are also found for the EA pattern.

Figure 9 presents the correlation maps for the significant relationships described in Table 4. The first EOF from RR and CWD and the EOF2 from CDD (contour lines, first row) show a northwest-southeast dipole that fits with the areas with significant correlation with the NAO (shaded regions). The NAO negative phases are related to more precipitation and CWD in the northwest of Europe and drought conditions in the

HESSD
10, 12331–12371, 2013

Balkans and Italy. EAWRUS is also related to precipitation in this season providing similar pattern as for the NAO but with smaller correlation values (figure not shown). The second EOF from RR and CWD (contour lines, second row) discriminates the southwest from the northeast, and that pattern is similar to the regions correlated with the SCAND pattern in summer. Mean precipitation and CWD (CDD) is positively (negatively) related to SCAND in the south, so negative phases of this index, would give droughts, for instance, in the Iberian Peninsula and the Balkans.

These highlighted regions are those presenting the most significant trends in summer (see Fig. 8), so drier conditions are related to the dynamical mechanisms behind the SCAND in the Iberian Peninsula and south of France, and they are also modulated by the NAO in Italy and Greece. The overall summer trend in the continent (east–west dipole) could be related to SCAND configuration. Composite maps for SLP are obtained for years with largest anomalies of CDD (PC2) and NAO (Fig. 10). At low level there is an opposite correspondence between the patterns of CDD and NAO in agreement with the correlation found in Table 4.

4.4 Autumn

The trend analysis in autumn indicates increasing significant trend for RR and CWD in the eastern Europe whereas CDD suffers a decrease in several regions in Central Europe and northwestern part of the Iberian Peninsula (Fig. 11). In contrast to the local changes in CWD and CDD, almost the whole continent presents an increase of very extreme precipitation (R95pTOT). Particularly, the changes in the Alpine region could be critical, since autumn is the most important season for heavy precipitation in this region (Schmidli et al., 2007).

The study of correlations with teleconnection patterns shows that the SCAND pattern is very significantly related to RR, CDD and CWD (Table 5). The very extreme precipitation (R95pTOT) is more related to the AMO. The SOI signal was found correlated with the second PC from the mean precipitation. Notice that only in spring and autumn the SOI is connected to precipitation over Europe and in particular over the

HESSD
10, 12331–12371, 2013

Iberian Peninsula, which is in agreement with other studies (Rocha, 1999; Frias et al., 2010). In autumn, el Niño events are associated to wetter conditions over the Iberian Peninsula.

Figure 12 shows the regionalization obtained for RR, CWD and CDD (contour lines represent the main EOFs from these variables according to the highest correlations shown in Table 5). The patterns plotted in the first row show a southwestern–northeastern configuration which fits with the areas where there is significant correlation with the SCAND pattern (shaded areas). Positive correlation with RR and CWD in the Iberian Peninsula and France and negative in the northeast of the continent imply that the SCAND positive phases are related to wetter autumns in the former regions and drier in the latter. The opposite is obtained for CDD and for this extreme the shaded region in the north is bigger than that for CWD, as it was in spring and summer. Significant correlations have also been obtained between the EAWRUS and RR, and the NAO and CDD (second row). The very extreme precipitation (R95pTOT) is positively correlated with the AMO over sparse areas through the continent (figure not shown).

Composite maps of sea surface temperature (SST) for the years with largest anomalies of R95pTOT (PC1) and AMO are shown in Fig. 13a and b respectively, indicating the pattern of positive influence of the AMO and El Niño on R95pTOT. According to Table 5, the linear relationship between the R95pTOT and el Niño is not significant. This may be a non linear relationship since it appears only for the most extreme events (positive SST anomaly over the Pacific in Fig. 13a). SST anomalies contribute to local variations of moisture and hence to an increase of R95pTOT. In autumn, the positive phases of the AMO and El Niño cause greater values of the R95pTOT over Europe. However, it is interesting to note that for the largest values of the AMO there is a negative SST anomaly over the equatorial Pacific (Fig. 13b). Further research is necessary to understand those differences.

5 Conclusions

This study examines the changes in some hydrological extremes such as very extreme precipitation (R95pTOT) and consecutive wet/dry days (CWD/CDD) in comparison against mean precipitation (RR) by using the pseudo-observations from E-OBS dataset. The hydrological extremes trends are more significant than those for mean precipitation, especially for R95pTOT, in agreement with the Clausius–Clapeyron relation that describes how a warmer atmosphere can hold more water vapor, which produces in turn more intense precipitation. The increase of R95pTOT in all seasons might be related to an intensification of the hydrological cycle associated with a warming related increase of atmospheric moisture content (see e.g. Schmidli et al., 2007 and references therein). Therefore, the increase of moisture due to warming (Trenberth, 2011) may cause stronger changes in convective precipitation than in large-scale precipitation.

Changes in precipitation and derived extreme indices were associated with climate dynamics to interpret the opposite trend found over different European regions. Therefore, we have considered the interactions between hydrological extremes and the modes of low frequency circulation.

In the trend analysis we have detected vulnerable regions through the continent. One of the most affected regions is the Iberian Peninsula, with an important decrease of both mean and CWD during the year except in autumn, when CWD and RR do not change but R95pTOT increases. In addition, CDD increases in winter and decreases in autumn. The geographical location of the Iberian Peninsula, between tropical and middle latitudes may be one of the causes of its vulnerability. In the center of the continent interesting results arose: while the number of consecutive wet days decreases in winter, the very extreme precipitation increases, especially in winter and summer. That is an important outcome since the region around the Alps is one of the places of the continent with the highest precipitation of Europe and that provides signals of climate change by hydrological extreme indices. Finally, in the north of Europe the positive

HESSD
10, 12331–12371, 2013

trend is more significant for extremes than for mean precipitation along the year, especially for R95pTOT.

Considering the continent as a whole, the trend analysis presents a different pattern in the extreme precipitation regime during the year (this agrees with the results found for RR by van den Besselaar et al., 2012). In winter, both mean precipitation and consecutive wet days present an upwards (downwards) trend in the north (south) of the continent, while in summer these two variables decrease (increase) in the west (east) of Europe. This seasonal behavior leads us to think that the atmospheric teleconnection patterns are responsible of these changes and they modulate the precipitation extremes in Europe. The very extreme precipitation index presents a positive trend during the year, so it is more reasonable to think that this is related to a longer period oscillation (i.e. the AMO).

The regionalization of hydrological indices divides Europe into two areas with different variability. In winter we obtained a north-south dipole, while northeast–southwest in spring and autumn and northwest-southeast in summer. As mentioned before, teleconnection patterns are considered to explain these differences. The influence of the teleconnection patterns is different for each season, being the NAO, EA, EAWRUS and SCAND the most relevant. In winter, the NAO present the strongest relation with both mean and extreme precipitation (CDD and CWD). In summer, we also found the most important relation with the NAO, but with opposite sign than that in winter. In spring and autumn, the SCAND, the EAWRUS and the EA affect the variability of the indices, with greater correlation coefficients in autumn. In both seasons, spring and autumn, precipitation shows the SOI influence over the Iberian Peninsula, but with opposite sign. An interesting result is the contribution of sea surface temperature of the Atlantic Ocean to explain the very extreme precipitation (R95pTOT) variability, since it was found the highest correlation with the Atlantic Multidecadal Oscillation (AMO), for all the seasons. At this point it is important to consider the different dynamical mechanisms that are behind each extreme event; what causes R95pTOT seems to depend on the sea surface temperature instead of the circulation weather regimes causing CWD/CDD.

The influence of water vapour variations on that indicator agrees with the findings of Zhang et al. (2013) about the relationships of the leading mode of water vapour with AMO and ENSO.

In summary, we obtained interactions between the interannual variability of hydrological indices and modes of low frequency circulation. Due to the limitations of global climate model outputs for hydrological applications, this work could pave the way of new possibilities for the projection of extremes under other climatic conditions. To clarify if future changes in extremes could be attributable to global warming we are performing studies to project the extreme indices from the found relationships with the large-scale processes. Detecting changes in extremes may help to improve the adaptation to a warming climate, especially with regard to crops.

Supplementary material related to this article is available online at http://www.hydrol-earth-syst-sci-discuss.net/10/12331/2013/hessd-10-12331-2013-supplement.pdf.

Acknowledgements. We acknowledge the free availability of the E-OBS dataset from the EU-FP6 project ENSEMBLES (http://ensembles-eu.metoffice.com) and the data providers in the ECA&D project (http://eca.knmi.nl), the CPC and the NCEP NOAA for the teleconnection indices. We also thanks the software developers of CDO (Climate Data Operators), CDAT (Climate Data Analysis Tool) and GrADS (Grid Analysis Display System).

This work is supported by projects EXTREMBLES (CGL2010-21869), CORWES (CGL2010-22158-C02), GCL2008-04610 and CGL2011-23209 from the Spanish R&D&I programme, SA222A11-2 regional project JCyL, and CLIM-RUN from the 7th European Framework Programme (FP7). A. Casanueva and N. González-Reviriego would like to thank the Spanish Government for the funding provided within the FPI programme.

References

Barnston, A. G. and Livezey, R. E.: Classification, seasonality and persistence of low-frequency atmospheric circulation patterns, Mon. Weather Rev., 115, 1083–1126, 1987. 12334

Bladé, I., Fortuny, D., van Oldenborgh, G., and Liebmann, B.: The summer North Atlantic Oscillation in CMIP3 models and related uncertainties in projected summer drying in Europe, J. Geophys. Res., 117, D16104, doi:10.1029/2012JD017816, 2012. 12344

Bueh, C. and Nakamura, H.: Scandinavian pattern and its climatic impact, Q. J. Roy. Meteor. Soc., 133, 2117–2131, 2007. 12336

Carril, A. F., Gualdi, S., Cherchi, A., and Navarra, A.: Heatwaves in Europe: areas of homogeneous variability and links with the regional to large-scale atmospheric and SSTs anomalies, Clim. Dynam., 30, 77–98, 2008. 12334

Dima, M. and Lohmann, G.: A hemispheric mechanism for the Atlantic Multidecadal Oscillation, J. Climate, 20, 2706–2719, doi:10.1175/JCLI4174.1, 2007. 12336

Donat, M., Alexander, L., Yang, H., Durre, H., Vose, R., and Caesar, J.: Global land-based datasets for monitoring climatic extremes, B. Am. Meteorol. Soc., 94, 997–1006, 2013. 12333

Easterling, D. R., Meehl, G. A., Parmesan, C., Changnon, S. A., Karl, T. R., and Mearns, L. O.: Climate extremes: observations, modeling, and impacts, Science, 289, 2068–2074, 2000. 12333

Enfield, D. B., Mestas-Nuñez, A., and Trimble, P.: The Atlantic multidecadal oscillation and its relationships to rainfall and river flows in the continental U.S., Geophys. Res. Lett, 28, 2077–2080, 2001. 12336

Frias, M. D., Herrera, S., Cofino, A. S., and Gutierrez, J. M.: Assessing the skill of precipitation and temperature seasonal forecasts in Spain: windows of opportunity related to ENSO events, J. Climate, 23, 209–220, 2010. 12336, 12346

Giorgi, F.: Climate change hot-spots, Geophys. Res. Lett., 33, L08707, doi:10.1029/2006GL025734, 2006. 12333

Haylock, M. R. and Goodess, C. M.: Interannual variability of European extreme winter rainfall and links with mean large-scale circulation, Int. J. Climatol., 24, 759–776, 2004. 12341

Haylock, M. R., Hofstra, N., Tank, A., Klok, E. J., Jones, P. D., and New, M.: A European daily high-resolution gridded data set of surface temperature and precipitation for 1950–2006, J. Geophys. Res.-Atmos., 113, D20119, doi:10.1029/2008JD010201, 2008. 12334, 12335

HESSD
10, 12331–12371, 2013

Hidalgo-Muñoz, J. M., Argueso, D., Gamiz-Fortis, S. R., Esteban-Parra, M. J., and Castro-Diez, Y.: Trends of extreme precipitation and associated synoptic patterns over the southern Iberian Peninsula, J. Hydrol., 409, 497–511, 2011. 12334

Hoerling, M. P. and Kumar, A.: Understanding and predicting extratropical teleconnections related to ENSO, in: El Niño and the Southern Oscillation: Multi-scale Variationsnd Global and Regional Impacts, edited by: Diaz, H. F. and Markgraf, V., Cambridge University Press, 57–88, 2000. 12336

Hofstra, N., Haylock, M., New, M., and Jones, P. D.: Testing E-OBS European high-resolution gridded data set of daily precipitation and surface temperature, J. Geophys. Res.-Atmos., 114, D21101, doi:10.1029/2009JD011799, 2009. 12335

IPCC: Summary for policymakers, in: Intergovernmental Panel on Climate Change Special Report on Managing the Risks of Extreme Events and Disasters to Advance Climate Change Adaptation, edited by: Field, C. B., Barros, V., Stocker, T. F., Qin, D., Dokken, D., Ebi, K. L., Mastrandrea, M. D., Mach, K. J., Plattner, G.-K., Allen, S., Tignor, M., and Midgley, P. M., Tech. rep., 2011. 12333

Jolliffe, I.: Principal Component Analysis, Springer, 2002. 12338

Kalnay, E., Kanamitsu, M., Kistler, R., Collins, W., Deaven, D., Gandin, L., Iredell, M., Saha, S., White, G., Woollen, J., Zhu, Y., Leetmaa, A., Reynolds, R., Chelliah, M., Ebisuzaki, W., Higgins, W., Janowiak, J., Mo, K., Ropelewski, C., Wang, J., Jenne, R., and Joseph, D.: The NCEP/NCAR 40-year reanalysis project, B. Am. Meteorol. Soc., 77, 437–471, 1996. 12337

Kendall, M. G.: Rank Correlation Methods, 4th Edn. Charles Griffin, London, 1975. 12338

Kostopoulou, E. and Jones, P.: Assessment of climate extremes in the Eastern Mediterranean, Meteorol. Atmos. Phys., 89, 69–85, 2005. 12334

Lorenz, E.: Empirical orthogonal functions and statistical weather prediction, Scientific Report 1, Statistical Forecasting Project, Department of Meteorology, Massachusetts Institute of Technology, Cambridge, Massachusetts, 1956. 12338

North, G., Bell, T., Cahalan, R., and Moeng, F.: Ampling errors in the estimation of empirical orthogonal functions, Mon. Weather Rev., 110, 699–706, 1982. 12339

Peterson, T. C., Heim, R., Hirsch, R., Kaiser, D., Brooks, H., Diffenbaugh, N., Dole, R., Giovannettone, J., Guirguis, K., Karl, T., Katz, R., Kunkel, K., Lettenmaier, D., McCabe, G., Paciorek, C., Ryberg, K., Schubert, S., Silva, V., Stewart, B., Vecchia, A., Villarini, G., Vose, R., Walsh, J., Wehner, M., Wolock, D., Wolter, K., Woodhouse, C., and Wuebbles, D.: Monitoring and

HESSD
10, 12331–12371, 2013

understanding changes in heat waves, cold waves, floods, and droughts in the united states: state of knowledge, B. Am. Meteorol. Soc., 94, 821–834, 2013. 12333
Ramos, A. M., Lorenzo, M. N., and Gimeno, L.: Compatibility between modes of low-frequency variability and circulation types: a case study of the northwest Iberian Peninsula, J. Geophys. Res.-Atmos., 115, D02113, doi:10.1029/2009JD012194, 2010. 12336
Rocha, A.: Low-frequency variability of seasonal rainfall over the Iberian Peninsula and ENSO, Int. J. Climatol., 19, 889–901, 1999. 12346
Rodo, X., Baert, E., and Comin, F.: Variations in seasonal rainfall in Southern Europe during the present century: relationships with the North Atlantic Oscillation and the El Niño-Southern Oscillation, Clim. Dynam., 13, 275–284, 1997. 12336
Rodríguez-Puebla, C., Encinas, A. H., and Sáenz, J.: Winter precipitation over the Iberian peninsula and its relationship to circulation indices, Hydrol. Earth Syst. Sci., 5, 233–244, doi:10.5194/hess-5-233-2001, 2001. 12336
Rodriguez-Puebla, C., Ayuso, S., Frias, M., and Garcia-Casado, L.: Effects of climate variation on winter cereal production in Spain, Clim. Res., 34, 223—232, 2007. 12334
Ropelewski, C. F. and Halpert, M. S.: Global and regional scale precipitation patterns associated with the El Niño/Southern Oscillation, Mon. Weather Rev., 115, 1606–1626, 1987. 12336
Schmidli, J., Goodess, M., C., Frei, C., Haylock, M. R., Hundecha, Y., Ribalaygua, J., and Schmith, T.: Statistical and dynamical downscaling of precipitation: an evaluation and comparison of scenarios for the European Alps, J. Geophys. Res., 112, D04105, doi:10.1029/2005JD007026, 2007. 12345, 12347
Schonwiese, C. D., Grieser, J., and Tromel, S.: Secular change of extreme monthly precipitation in Europe, Theor. Appl. Climatol., 75, 245–250, 2003. 12333, 12334
Sen, P. K.: Estimates of regression coefficient based on Kendalls Tau, J. Am. Stat. Assoc., 63, 1379–1389, doi:10.2307/2285891, 1968. 12338
Tank, A. and Konnen, G. P.: Trends in indices of daily temperature and precipitation extremes in Europe, 1946–99, J. Climate, 16, 3665–3680, 2003. 12333
Tebaldi, C., Hayhoe, K., Arblaster, J. M., and Meehl, G. A.: Going to the extremes: an intercomparison of model simulated historical and future changes in extreme events, Climatic Change, 3–4, 185–211, 2006. 12333
Trenberth, K. E.: Changes in precipitation with climate change, Clim. Res., 47, 123–138, 2011. 12333, 12347

Trigo, R. M., Pozo-Vazquez, D., Osborn, T. J., Castro-Diez, Y., Gamiz-Fortis, S., and Esteban-Parra, M. J.: North Atlantic oscillation influence on precipitation, river flow and water resources in the Iberian Peninsula, Int. J. Climatol., 24, 925–944, 2004. 12336

van den Besselaar, E. J. M., Klein Tank, A. M. G., and Buishand, T. A.: Trends in European precipitation extremes over 1951–2010, Int. J. Climatol., 33, 2682–2689, doi:10.1002/joc.3619, 2012. 12333, 12340, 12344, 12348

Vicente-Serrano, S., Beguería, S., López-Moreno, J., El Kenawy, A., and Angulo, M.: Daily atmospheric circulation events and extreme precipitation risk in Northeast Spain: the role of the North Atlantic oscillation, Western Mediterranean oscillation, and Mediterranean oscillation, J. Geophys. Res.-Atmos., 114, D08106, doi:10.1029/2008JD011492, 2009. 12334, 12336

von Storch, H. and Zwiers, F.: Statistical Analysis in Climate Research, Cambridge University Press, Cambridge, 1999. 12339

Wallace, J. M. and Gutzler, D. S.: Teleconnections in the geopotential height field during the Northern Hemisphere winter, Mon. Weather Rev., 109, 784–812, 1981. 12336

Wilks, D.: Statistical methods in the atmospheric sciences, 2nd Edn., Academic Press, 2006. 12338

Zhang, L., Wu, L., and Gan, B.: Modes and mechanisms of global water vapor variability over the twentieth century, J. Climate, 26, 5578–5593, doi:10.1175/JCLI-D-12-00585.1, 2013. 12349

Zhang, R. and Delworth, T. L.: Impact of Atlantic multidecadal oscillations on India/Sahel rainfall and Atlantic hurricanes, Geophys. Res. Lett., 33, L17712, doi:10.1029/2006GL026267, 2006. 12336

Zorita, E., Kharin, V., and von Storch, H.: The Atmospheric circulation and sea-surface temperature in the North-Atlantic area in winter – their interaction and relevance for Iberian precipitation, J. Climate, 5, 1097–1108, 1992. 12336

Zveryaev, I.: Seasonally varying modes in long-term variability of European precipitation during the 20th century, J. Geophys. Res.-Atmos., 111, D21116, doi:10.1029/2005JD006821, 2006. 12336

Table 1. Extreme indicators considered in the study.

Acronym	Definition	Unit
CWD	Largest number of consecutive wet days	days
CDD	Largest number of consecutive dry days	days
R95pTOT	Quotient of the precipitation in days where daily precipitation exceeds the 95th percentile of the reference period and the total amount of precipitation	%

HESSD
10, 12331–12371, 2013
Extreme precipitation and teleconnections in Europe
A. Casanueva et al.

Table 2. Correlation coefficients between the leading PCs of mean and extreme precipitation and the teleconnection indices in winter. The variance of each principal component is shown in brackets. Only significant values are shown.

	NAO	EA	EAWRUS	SCAND	AMO
RR-PC1 (39 %)	-0.68 ± 0.06[b]	0.34 ± 0.11[b]	-0.48 ± 0.09[b]	0.51 ± 0.09[b]	–
RR-PC2 (16 %)	0.32 ± 0.12[a]	0.52 ± 0.09[b]	-0.29 ± 0.11[a]	–	–
CDD-PC1 (26 %)	0.56 ± 0.11[b]	–	0.56 ± 0.07[b]	-0.47 ± 0.09[a]	–
CDD-PC3 (8 %)	–	-0.47 ± 0.09[b]	–	–	–
CWD-PC1 (22 %)	-0.73 ± 0.06[b]	–	-0.45 ± 0.09[b]	0.54 ± 0.09[a]	–
CWD-PC2 (13 %)	–	0.55 ± 0.09[b]	-0.45 ± 0.10[b]	–	–
R95pTOT-PC1 (17 %)	–	–	–	–	0.54 ± 0.09[b]
R95pTOT-PC3 (4 %)	0.41 ± 0.10[b]	–	–	-0.33 ± 0.13[b]	–

[a] p value < 0.05.
[b] p value < 0.01.

HESSD
10, 12331–12371, 2013
Extreme precipitation and teleconnections in Europe
A. Casanueva et al.

Table 3. As Table 2, but for spring.

	SCAND	EA	SOI	AMO
RR-PC2 (16 %)	0.48 ± 0.11[b]	−0.33 ± 0.14[b]	0.39 ± 0.11[b]	–
CDD-PC1 (17 %)	−0.26 ± 0.13[a]	–	–	–
CDD-PC2 (13 %)	0.44 ± 0.12[b]	–	0.40 ± 0.08[b]	–
CWD-PC1 (17 %)	–	−0.38 ± 0.11[b]	–	–
CWD-PC2 (10 %)	0.47 ± 0.10[b]	–	0.33 ± 0.12[b]	–
R95pTOT-PC1 (18 %)	–	–	–	0.52 ± 0.09[b]
R95pTOT-PC2 (5 %)	–	–	–	0.50 ± 0.10[b]

HESSD
10, 12331–12371, 2013

HESSD
10, 12331–12371, 2013
Extreme precipitation and teleconnections in Europe
A. Casanueva et al.

Table 4. As Table 2, but for summer.

	NAO	EA	EAWRUS	SCAND	AMO
RR-PC1 (19 %)	0.68 ± 0.06^b	-0.46 ± 0.12^b	0.39 ± 0.10^b	0.26 ± 0.12^a	–
RR-PC2 (14 %)	–	–	–	0.51 ± 0.10^b	–
CDD-PC1 (22 %)	–	–	–	-0.33 ± 0.07^b	-0.30 ± 0.10^a
CDD-PC2 (15 %)	-0.58 ± 0.07^b	0.49 ± 0.11^b	-0.37 ± 0.10^b	-0.48 ± 0.10^b	0.26 ± 0.12^a
CWD-PC1 (19 %)	0.68 ± 0.06^b	-0.35 ± 0.13^b	0.37 ± 0.10^b	0.29 ± 0.12^a	–
CWD-PC2 (8 %)	–	–	–	0.37 ± 0.13^b	–
R95pTOT-PC1 (10 %)	–	-0.40 ± 0.09^b	–	–	-0.53 ± 0.08^b
R95pTOT-PC2 (7 %)	–	0.43 ± 0.11^b	–	–	–

Table 5. As Table 2 for autumn.

	NAO	EA	EAWRUS	SCAND	SOI	AMO
RR-PC1 (26 %)	-0.35 ± 0.13^{b}	–	–	0.71 ± 0.07^{b}	–	–
RR-PC2 (14 %)	–	–	0.37 ± 0.13^{b}	0.27 ± 0.12^{a}	-0.30 ± 0.08^{b}	–
CDD-PC1 (20 %)	0.44 ± 0.09^{b}	–	0.30 ± 0.14^{a}	–	–	–
CDD-PC2 (15 %)	0.27 ± 0.15^{a}	–	–	-0.64 ± 0.07^{a}	–	-0.37 ± 0.10^{b}
CWD-PC1 (16 %)	-0.27 ± 0.12^{a}	0.35 ± 0.12^{b}	-0.26 ± 0.11^{a}	0.38 ± 0.12^{b}	–	–
CWD-PC2 (12 %)	–	–	–	0.67 ± 0.07^{b}	–	–
R95pTOT-PC1 (16 %)	–	–	–	0.32 ± 0.11^{a}	–	0.64 ± 0.08^{b}

HESSD
10, 12331–12371, 2013

Extreme precipitation and teleconnections in Europe

A. Casanueva et al.

HESSD
10, 12331–12371, 2013

Extreme precipitation and teleconnections in Europe

A. Casanueva et al.

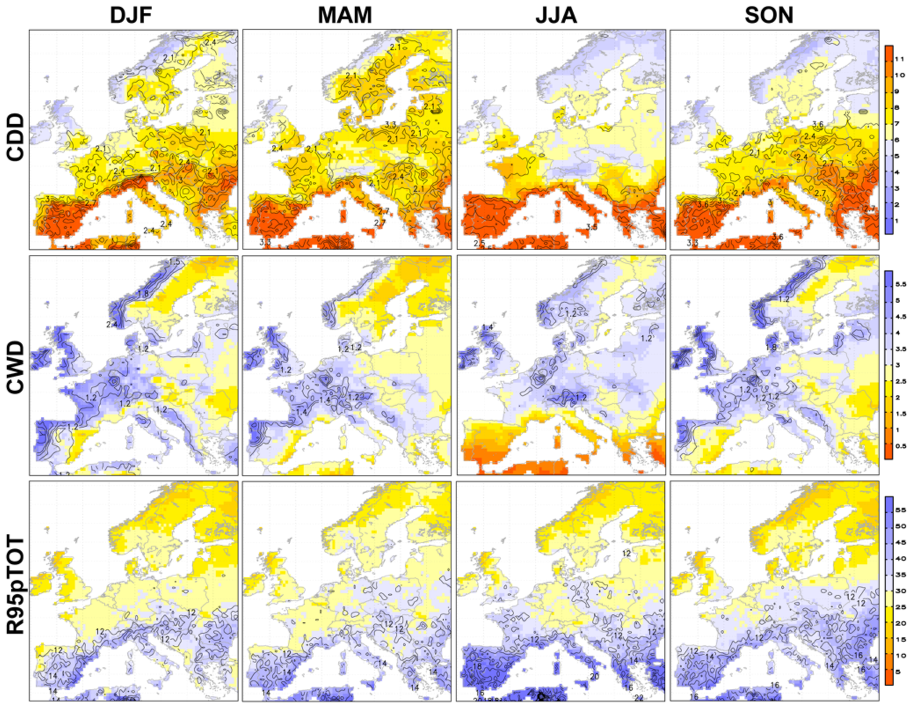

Fig. 1. Seasonal mean distribution of CDD (days), CWD (days) and R95pTOT (%) in shading. Contour lines represent the standard deviation for each indicator and season.

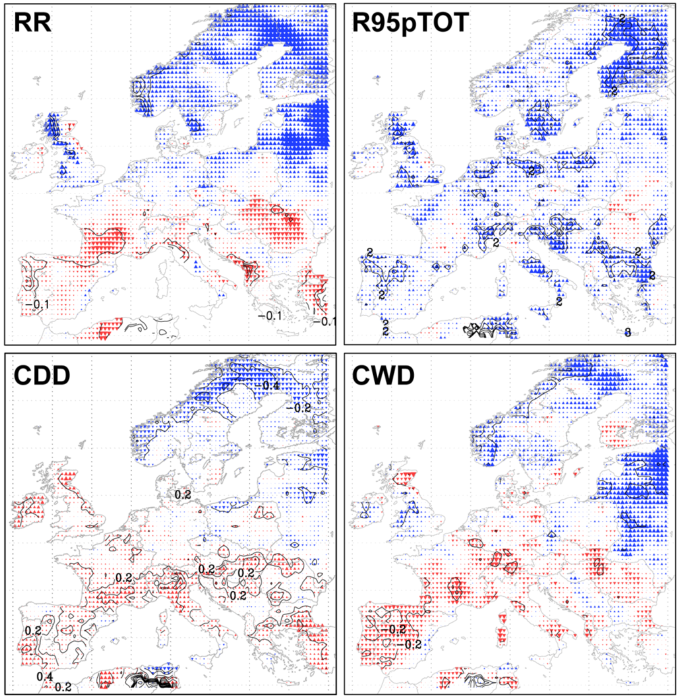

Fig. 2. Trend maps of RR, CDD, CWD and R95pTOT in winter. Downward-pointing (upward-pointing) triangles indicate a decreasing (increasing) trend. Their size is proportional to trend significance. Only significant values at 5 % are plotted. Black contour lines represent the Sen's slope per decade.

HESSD
10, 12331–12371, 2013

Extreme precipitation and teleconnections in Europe

A. Casanueva et al.

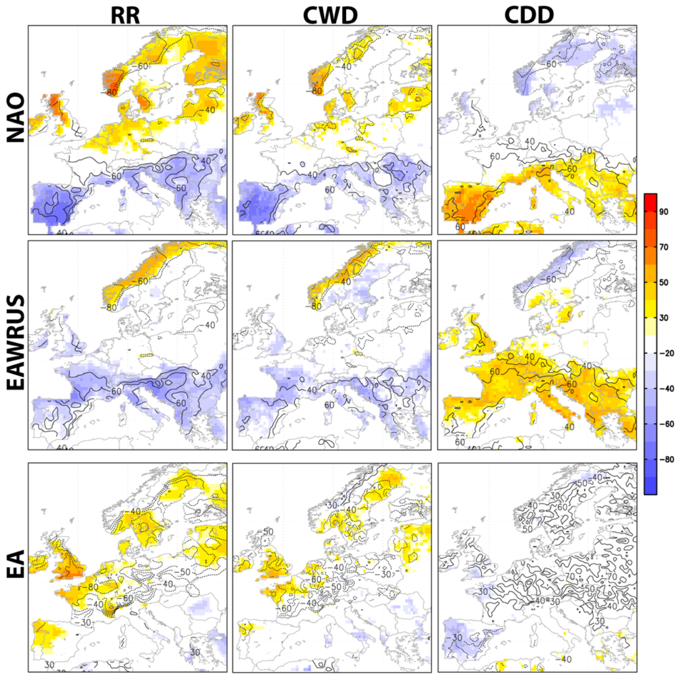

Fig. 3. Shaded regions represent the correlation coefficients (×100) between the teleconnection indices (NAO, EAWRUS, EA by rows) and the daily mean or extreme precipitation fields (by columns) in winter. Contour lines represent the EOF associated to the PC better correlated with the teleconnection index according to Table 2.

HESSD
10, 12331–12371, 2013

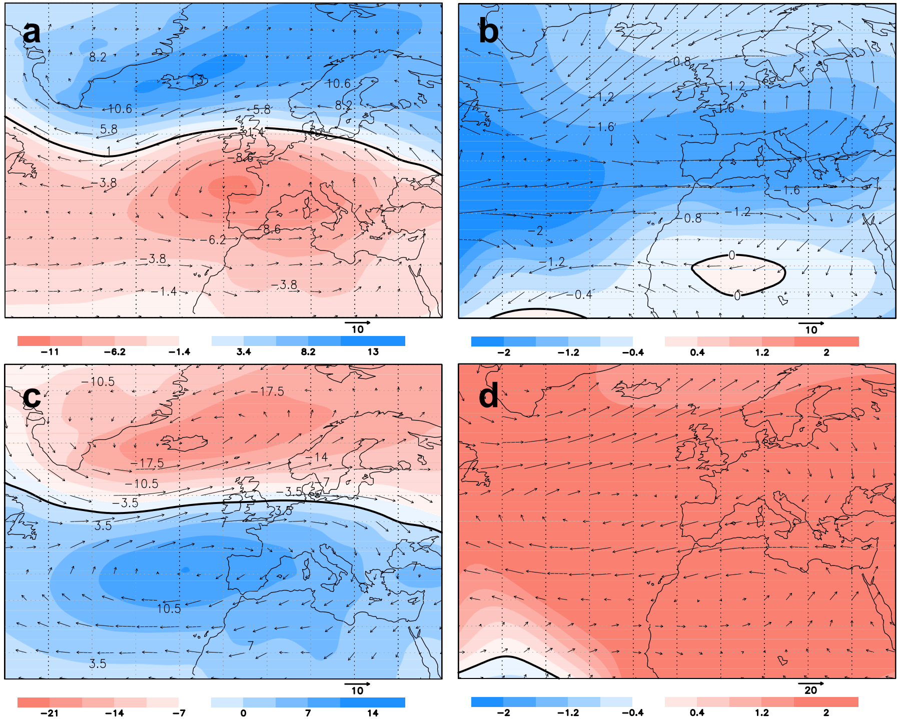

Fig. 4. Composite maps of SLP (hPa) and wind ($m\,s^{-1}$) at 850 hPa **(a)** and velocity potential ($\times 10^6\,m^2\,s^{-1}$) at 200 hPa **(b)** for extreme CWD (PC1) in winter. Same maps for the NAO (**c** and **d**).

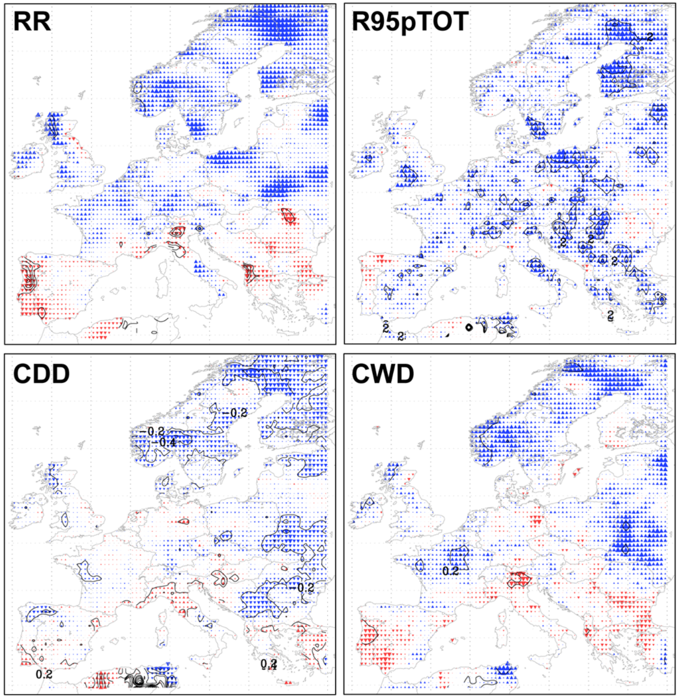

Fig. 5. As in Fig. 2, but for spring.

HESSD
10, 12331–12371, 2013

Extreme precipitation and teleconnections in Europe

A. Casanueva et al.

Title Page
Abstract | Introduction
Conclusions | References
Tables | Figures
◀| |▶
◀ ▶
Back | Close
Full Screen / Esc
Printer-friendly Version
Interactive Discussion

HESSD
10, 12331–12371, 2013

Extreme precipitation and teleconnections in Europe

A. Casanueva et al.

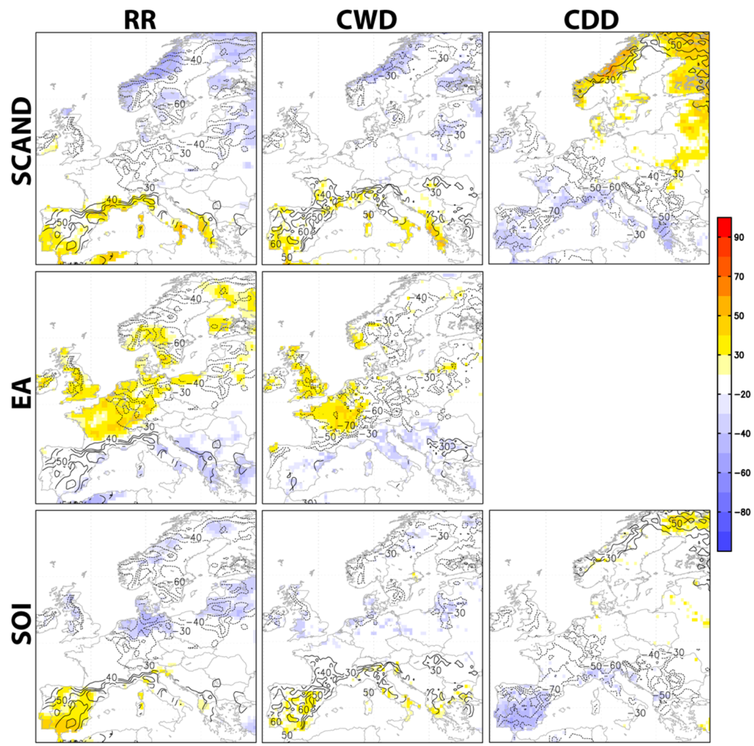

Fig. 6. Shaded regions represent the correlation coefficients (×100) between the teleconnection indices (SCAND, EA, SOI by rows) and the mean or extreme precipitation field (by columns) in spring. Contour lines represent the EOF associated to the PC better correlated with the teleconnection index according to Table 3.

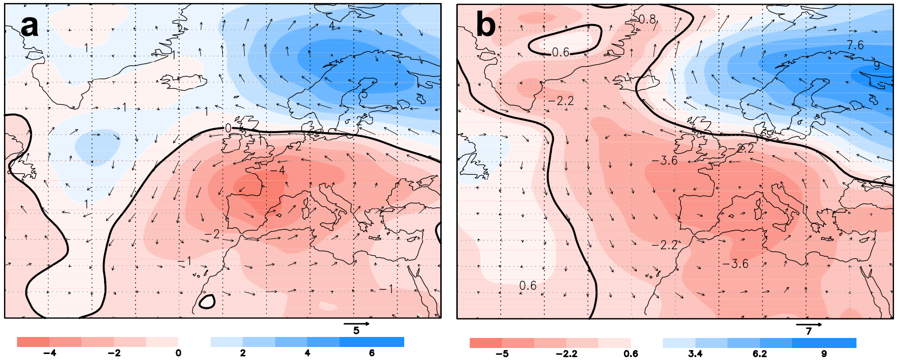

Fig. 7. Composite maps of SLP (hPa) and wind ($m\,s^{-1}$) at 850 hPa for CWD (PC2) **(a)** and for the SCAND **(b)** in spring.

HESSD
10, 12331–12371, 2013

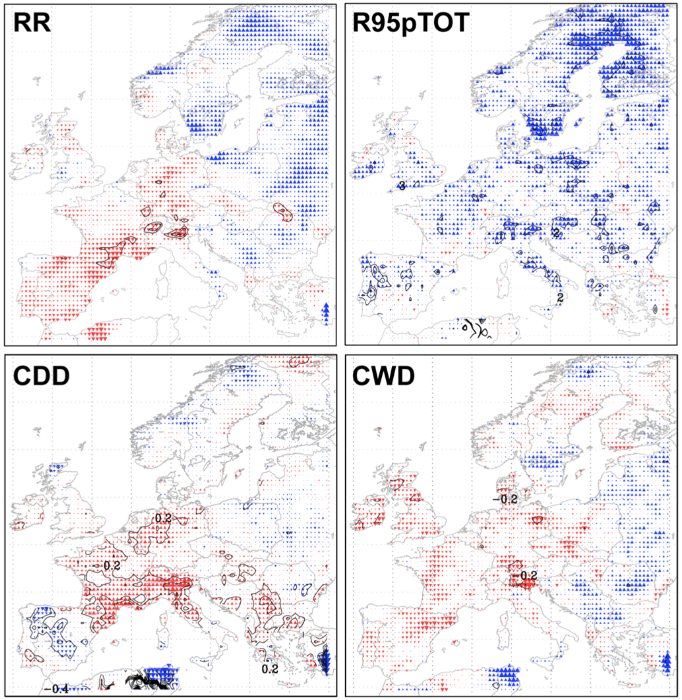

Fig. 8. As in Fig. 2, but for summer.

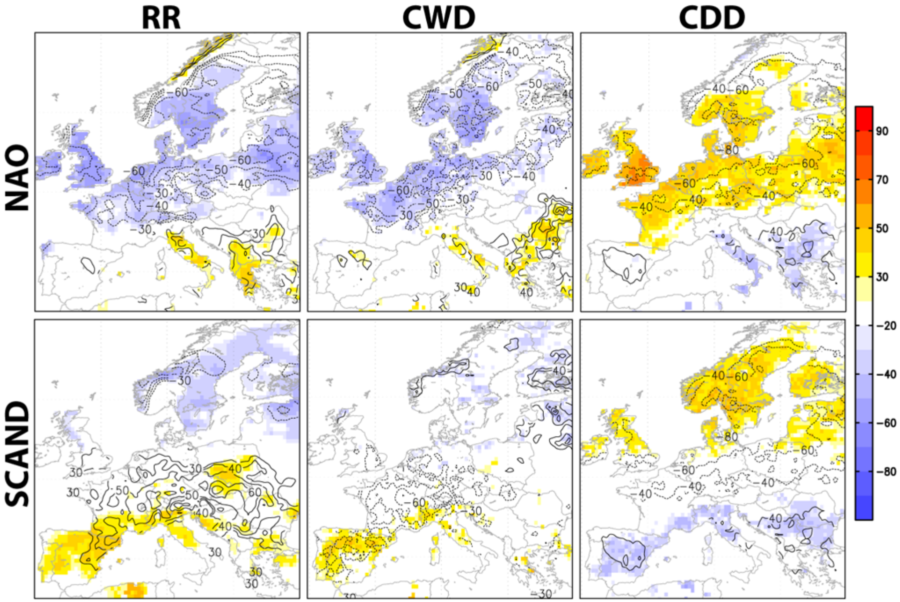

Fig. 9. Shaded regions represent the correlation coefficients (×100) between the teleconnection indices (NAO, SCAND, by rows) and the daily mean or extreme precipitation fields (by columns) in summer. Contour lines represent the EOF associated to the PC better correlated with the teleconnection index according to Table 4.

HESSD
10, 12331–12371, 2013

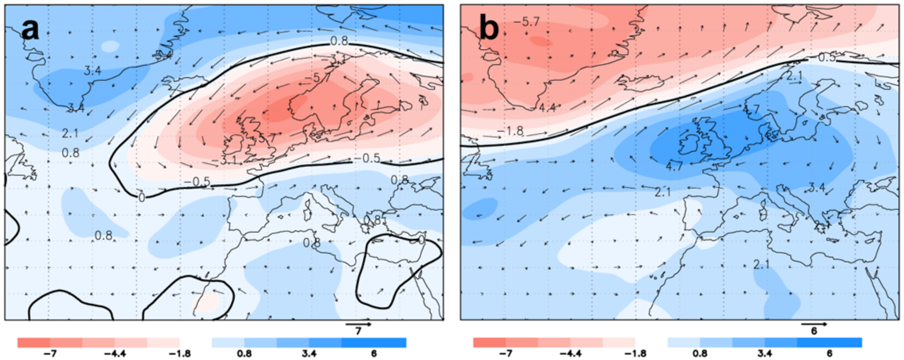

Fig. 10. Composite maps of SLP (hPa) and wind ($m\,s^{-1}$) at 850 hPa for CDD (PC2) **(a)** and for the NAO **(b)** in summer.

HESSD

10, 12331–12371, 2013

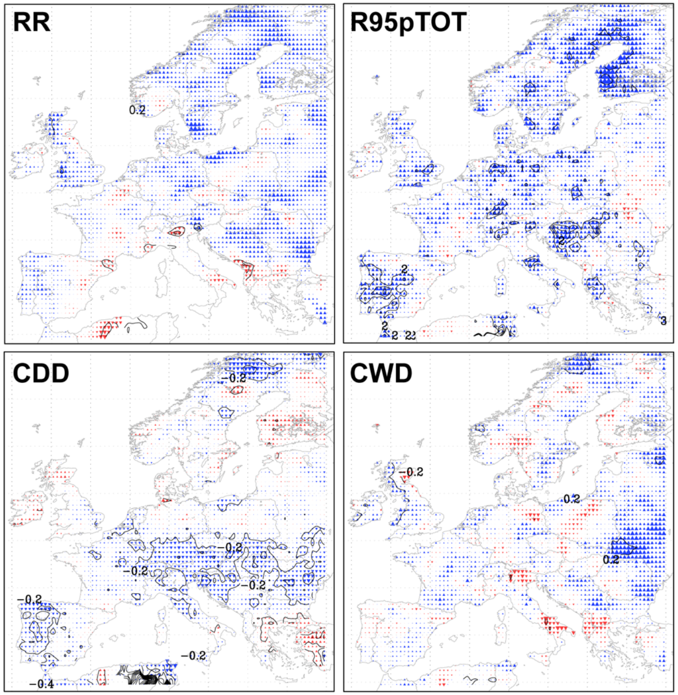

Fig. 11. As in Fig. 2, but for autumn.

HESSD
10, 12331–12371, 2013

Extreme precipitation and teleconnections in Europe

A. Casanueva et al.

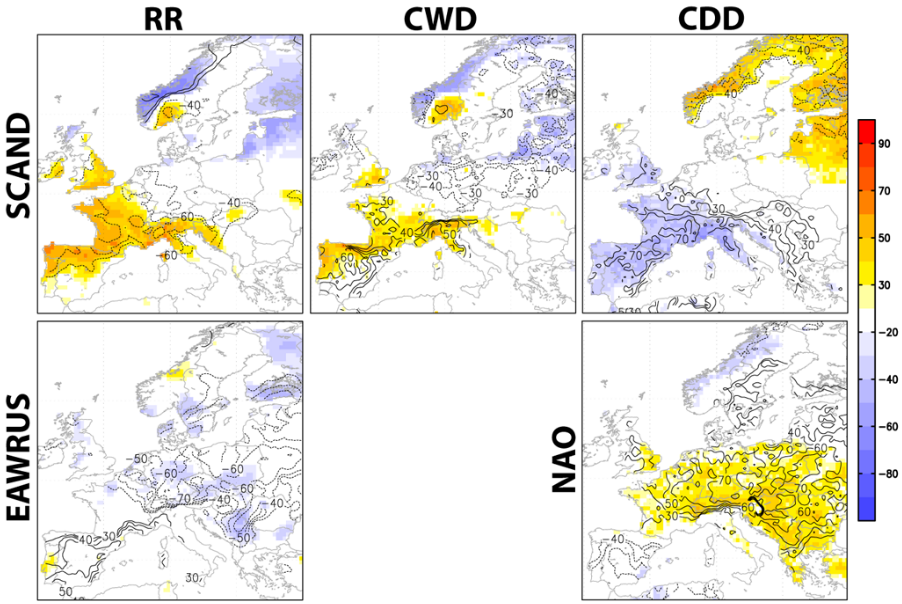

Fig. 12. Shaded regions represent the correlation coefficients (×100) between the teleconnection indices (SCAND, EAWRUS, NAO, by rows) and the daily mean or extreme precipitation fields (by columns) in autumn. Contour lines represent the EOF associated to the PC better correlated with the teleconnection index according to Table 5.

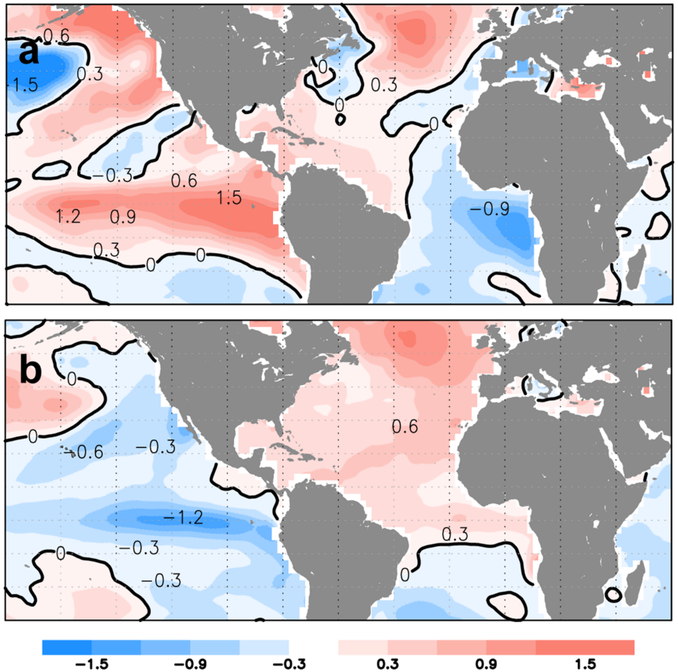

Fig. 13. Composite maps of SST for R95pTOT (PC1) **(a)** and for the AMO **(b)** in autumn.

HESSD
10, 12331–12371, 2013